Formation of Microporous Polymer Fibers and Oriented Fibrils by Precipitation with a Compressed Fluid Antisolvent

DAVID J. DIXON* and KEITH P. JOHNSTON†

Department of Chemical Engineering, University of Texas at Austin, Austin, Texas 78712

SYNOPSIS

Polymer morphology is controlled over a continuum from microspheres to interconnected bicontinuous networks to fibers with a versatile new process: precipitation with a compressed fluid antisolvent. The results are explained qualitatively as a function of phase behavior, mass-transfer pathways, and the formation rates of skin on the flowing jet. By spraying dilute polystyrene in toluene solutions into liquid carbon dioxide, extremely small 100 nm microspheres are formed. For concentrations above the critical composition, fibers are produced that are not only microcellular, but, in some instances, even hollow. Mass-transfer pathways that cross the binodal near the critical composition produce interconnected networks, likely due to spinodal decomposition. In this region, fibers composed of highly oriented microfibrils are produced at high shear rates. Preaddition of CO_2 influences the morphology because of dilution, in a similar manner as a liquid antisolvent, except that the viscosity reduction is larger due to added free volume. Because CO_2 diffuses through the glassy polystyrene skin faster than does a conventional liquid antisolvent such as methanol, it produces more porous fibers, which are also more cylindrical. © 1993 John Wiley & Sons, Inc.

INTRODUCTION

A variety of physical techniques may be used to form polymeric materials such as microspheres, porous membranes, hollow and porous fibers, and microcellular foams. For example, a liquid polymer solution may be cooled rapidly in a technique called thermally induced phase separation (TIPS) to produce each of these morphologies.[1-4] Phase separation may also be accomplished by addition of a liquid antisolvent.[5,6] Two additional techniques are based on the use of highly compressed gases or supercritical fluids. In a process called rapid expansion from supercritical solution (RESS), a dilute solution is expanded through a nozzle to generate a high degree of supersaturation, leading to fine, uniform microspheres or microfibers.[7-9] Mathematical models of the fluid mechanics have been presented for RESS.[10,11]. In the second technique, a microcellular foam is produced by heating or decompressing a polymer saturated with a gas such as CO_2, to cause nucleation and growth.[12,13]

Recently, a new process has been introduced in which polymer microspheres and fibers are produced by precipitation with a compressed fluid antisolvent (PCA).[14,15] Here, a polymer in a liquid solvent is sprayed across a small capillary into a vessel containing a compressed gas, liquid, or supercritical fluid, such as CO_2. CO_2 is miscible with the solvent, e.g., toluene, but is an antisolvent for the polymer. CO_2 may be somewhat soluble in the polymer, but the polymer solubility in the CO_2 is negligible. Thus, CO_2 is called an antisolvent in this work. Uniform amorphous polystyrene microspheres have been formed with diameters from 0.1 to 20 μm, as a function of the CO_2 temperature and density. Fibers with and without microporosity are obtained at 5 wt % polymer concentrations. These results were explained qualitatively in terms of mass transfer pathways, phase behavior, and jet behavior. A full model of the fluid mechanics and mass transport is not yet available, due to the very complex nature of compressible viscoelastic flow. Recently, Randolph et al.[16] formed sub-micron sized particles of poly(L-lactic acid) by spraying a methylene chloride solution into CO_2, relating particle diameter to the mass-transfer rates.

The objective of this study was to understand how various morphologies are formed in the PCA process from polymer discrete microspheres to spinodal bicontinuous structures to polymer continuous fibers. The key variables are the polymer concentration, spray conditions, and temperature and pressure (or

† To whom correspondence should be addressed.

* Present address: Dept. of Chemistry and Chemical Engineering, South Dakota School of Mines and Technology, Rapid City, SD 57701

Journal of Applied Polymer Science, Vol. 50, 1929-1942 (1993)

 CCC 0021-8995/93/111929-14

the density) of the antisolvent. We focus in detail on hollow and porous microcellular fibers and then on spinodal structures, to complement an earlier study that emphasized microspheres and particles.[15] The Results section begins with viscosity and phase behavior measurements, which are useful for explaining how the various polymer morphologies are produced. To further place the results in perspective, control experiments have been performed with liquid methanol as the antisolvent. Finally, we present an analysis of how CO_2's faster diffusion rates in glassy polymers affects the final polymer morphology.

The PCA process offers unique advantages compared with other techniques including spray drying and phase separation with liquid antisolvents. Thermally labile substances may be treated, unlike the case for spray drying at elevated temperatures. Also, diffusion coefficients of organic solvents in supercritical CO_2 are typically 1–2 orders of magnitude higher than in conventional liquid antisolvents.[17-19] Consequently, new mass transfer pathways are accessible. The density of the fluid may be tuned to influence the product morphology by altering jet breakup, phase behavior, and mass-transfer pathways. Supercritical CO_2 may be used to dry the polymer product rapidly without collapse of the structure due to capillary forces during depressurization, since a liquid–vapor interface is not present. Recovery of the CO_2 from the solvent is simpler than for liquid antisolvents. Often, higher polymer concentrations may be sprayed than in the RESS process due to higher polymer solubilities in a liquid solvent vs. a supercritical fluid. CO_2 may be added to the feed solution to lower viscosities, not only by acting as a diluent, but by incorporating additional free volume into the solution.[20] Thus, more concentrated solutions may be sprayed. Another advantage of CO_2 is its low toxicity. It can replace toxic solvents in applications such as controlled drug release. For example, a recently described process encapsulates drugs into polymers by a form of CO_2-induced precipitation.[21] CO_2 can swell amorphous polymers markedly, and, in addition, it has been shown to reduce significantly the glass transition temperature (T_g).[22] This reversible plasticization facilitates diffusion of solutes in polymers. Indeed, PCA offers many potential advantages for making a variety of polymeric materials to more than offset the disadvantage of elevated pressures. There are interesting applications for these materials. Polymer microspheres are of interest in chromatography, as adsorbents, and as supports for catalysts or impregnated materials such as drugs. Microcellular foams and fibers are of interest as membranes, filters, porous electrodes, high impact strength parts, and insulation.

THEORY

Figure 1 shows schematically various PCA mass-transfer pathways for a ternary system consisting of an amorphous polymer, an organic solvent, and a compressed fluid antisolvent. Between the binodal and spinodal curve is the metastable region. In this region, the system is stable to small concentration fluctuations, and the phase-separation mechanism is by nucleation and growth. For most high molecular weight polymers ($M_w > 10^4$), the critical point occurs at a volume fraction of polymer of 0.05 or less.[6] On the polymer-lean side of the critical composition or plait point, as the pathway enters the binodal, a polymer-rich phase nucleates and grows in a solvent-rich phase (path A). On the polymer-rich side of the plait point, the solvent and antisolvent mixture nucleates and grows in a polymer-rich phase (path C). Especially in the region near the critical point, the metastable region is very narrow (see path B), and it actually disappears at the critical point. If the pathway moves through this narrow region quickly, there is little time for nucleation and growth. At the spinodal curve, the solution will then separate by spinodal decomposition, resulting in a bicontinuous interconnected network of polymer and voids. Inferring spinodal decomposition from final polymer morphology may be difficult since coarsening (or ripening) of the spinodal network can occur.[3] Coarsening is caused by diffusion of polymer and solvent that lowers free energy by decreasing the interfacial area. Thus, if sufficient coarsening occurs before the spinodal network is quenched, or locked in by vitrification of the polymer, the morphologies formed by either spinodal decomposition or nucleation and growth may begin to look similar.

The porosity of polymer particles formed in an antisolvent process may be explained by mass-

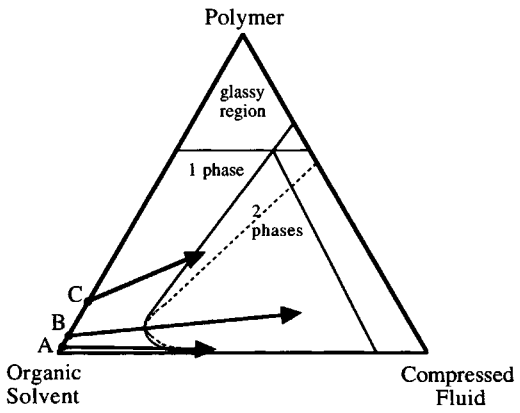

Figure 1 Schematic ternary diagram comparing different precipitation schemes with a compressed fluid antisolvent: (———) binodal curve, (----) spinodal curve.

transfer pathways on a ternary diagram (see Fig. 2).[23] Path [a] illustrates a case where the antisolvent mass-transfer rate into the polymer–solvent droplet (or fiber) is faster than that of the leaving solvent. When the solvent and antisolvent mass-transfer rates are approximately the same, then a path similar to [b] is followed. However, if the solvent mass-transfer rate is faster than the entering antisolvent rate, a more upward trajectory [c] is followed. The final polymer–antisolvent composition is indicative of the porosity of the polymer particle. If the phase diagram is known as well as the final composition, then the porosity can be estimated using the lever rule. The closer the final composition is to the antisolvent vertex, the more porous the material. Thus, the product produced by path [a] is more porous than by path [b], which, in turn, is more porous than by path [c].

Path [d] depicts an example where antisolvent is added into the polymer solution prior to spraying. The initial polymer solution is closer to phase separation or the binodal curve, but is still in the one-phase region. Here, less additional antisolvent will be needed to diffuse into the sprayed solution to cause precipitation. If the added antisolvent is a compressed fluid, it may also expand after spraying, leading to increased porosity and perhaps larger pores.

EXPERIMENTAL

Polystyrene (Scientific Polymer Products, M_w = 280,000, M_w/M_n = 2.37, or Pressure Chemicals, M_w = 200,000, M_w/M_n = 1.05) in toluene (Fischer, ACS grade) solutions were made with polystyrene concentrations from 1 to 25.8 wt %. The experimental apparatus included a horizontal view cell, which has been described along with the procedure

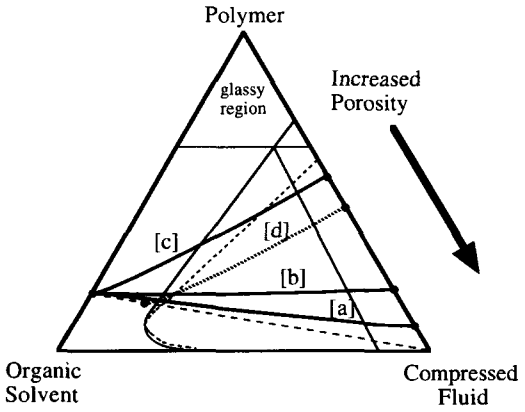

Figure 2 Schematic ternary diagram comparing mass-transfer pathways for precipitation with a compressed fluid antisolvent: (———) binodal curve, (----) spinodal curve).

in detail in a previous article.[15] Compositions from 1 to 6% were sprayed through a 100 μm i.d. 17.4 cm-long fused silica capillary tube, which had a polyimide coating. Compositions from 8 to 25.8% were sprayed through a 151 μm i.d. × 18 cm-long capillary tube. The larger diameter was needed primarily because of the higher solution viscosities. For these concentrations, a new vertical cell was developed to prevent particle agglomeration, by providing for an increased falling distance for the polymer before it touched either the wall of the cell or other wet polymer particles on the bottom.

The experimental setup for the vertical cell is shown schematically in Figure 3. The spray chamber consisted of an Autoclave Engineers (AE) medium-pressure tube, 2.54 cm o.d. × 1.746 cm i.d. × 20.32 cm long (Model CNLX 1608–316), rated to 689 bar. To facilitate recovery of the precipitated polymer, a 0.2 μm cellulose filter was inserted in the bottom coupling. The bottom vent valve was a stainless-steel needle valve (Whitey, SS-31RS4). During rapid purging of the cell, heating tape was required to prevent icing of the valve. One minor drawback of using the 8 in. cell, when compared with using a view cell, was that neither the precipitation nor spray could be viewed. This inconvenience was minimized by first observing the spray in a clear sapphire tube.

The system was equilibrated for 15–30 min., after which the solution was sprayed. The vent valve was then opened to sweep CO_2 through the cell to dry the polymer while the pressure was maintained at a constant value. After approximately 50 min. of purging with CO_2, the system was slowly depressurized over a 30 min. period, at the experimental temperature. It was not necessary to use supercritical fluid drying for the glassy fibers, as they did not collapse during depressurization. In some of the experiments, CO_2 was preadded into the polymer solution prior to spraying. Separate visual experiments in a view cell confirmed that the polymer solution with added CO_2 was well mixed within 15–30 minutes.

A variable volume view cell (2 in. o.d. × 11/16 in. i.d., 28 mL total internal volume) was used to determine the phase behavior of the polystyrene, toluene, and CO_2 system. This cell and procedure have been described in detail previously.[24,25] A weighed amount of polymer solution (±0.0001 g), with a known concentration of polystyrene in toluene, was added directly into the cell. The desired amount of CO_2 was loaded into the view cell by use of a syringe pump to within ±0.03 cm^3 (at 22°C and 139 bar).

The pressure in the view cell was adjusted to a constant value (60 bar) by use of a second syringe

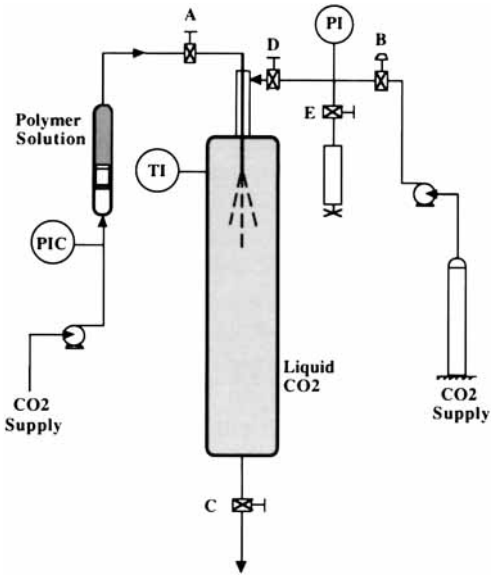

Figure 3 Apparatus for precipitation of polymer particles and fibers with a compressed fluid antisolvent (PCA).

pump and the piston in the back of the view cell. The magnetic stirrer caused rapid equilibration, typically within ~15–30 min. After equilibration, if phase separation had not occurred, then additional CO_2 was added. A point on the binodal curve was identified visibly when a phase separation occurred that did not disappear after at least 1 h of stirring and equilibration.

At high shear rates, typical of PCA experimental spray conditions, a capillary tube of known dimensions was used to determine the solution viscosity. The time required to collect a measured amount of polymer solution in a small capped vial for a specific ΔP was recorded. The amount of polymer solution collected was weighed to within 0.0001g. Three replicate experiments were made for each solution and the flow rate was averaged. The pressure drop across the tube was measured with an accuracy of ±0.7 bar. The non-Newtonian viscosity was calculated using the Weissenberg-Rabinowitsch equation, neglecting end effects,[26] and the reproducibility was ~2%.

RESULTS AND DISCUSSION

Viscosity Measurement

Solutions of polystyrene and toluene exhibit shear-thinning behavior under PCA flow conditions. Figure 4 is a summary showing how concentration and shear rate affect the non-Newtonian viscosity of polystyrene solutions in the power-law region. The power-law equation can be written as

$$\eta = m(\dot{\gamma}_R)^{n-1} \quad (1)$$

where η has units of g/cm/s and parameters m and n are reported in Table I. As concentration is increased, the viscosity increases as correlated with a fourth order polynomial equation for a specific rate of shear.[14] The effect of preadding CO_2 prior to spraying shows that a dramatic decrease in viscosity occurs. For the 12.8% polystyrene in toluene solution with CO_2 preadded, the actual polystyrene concentration was 10.85 wt%. The measured viscosity is 0.142 g/cm/s, at a shear rate of 1.301×10^5 (s^{-1}). From eq. (1) and Table I, a 12.8% polystyrene in toluene solution has a viscosity of 0.241 g/cm/s, at the same shear rate. CO_2 reduces the polystyrene solution viscosity by about 41%. This reduction is due in part to dilution; however, it is possible that this reduction is also caused by an increase in the free volume. From the above fourth-order correlation at the same shear rate, the viscosity of a 10.85% polystyrene in the toluene solution is calculated as 0.186 g/cm/s. This value is ~31% higher than for the solution at the same concentration including preadded CO_2. The difference is attributed to addition of freevolume to the solution by CO_2. Garg et al.[20] predicted the dilution and free-volume effects in a polydimethylsiloxane (PDMS) melt–CO_2 system.

Phase Behavior

The phase behavior plays a vital role in the PCA process. A full determination of the binodal curve for the polystyrene–toluene–CO_2 system is beyond the scope of this study; however, a few points were measured for polymer concentrations near the crit-

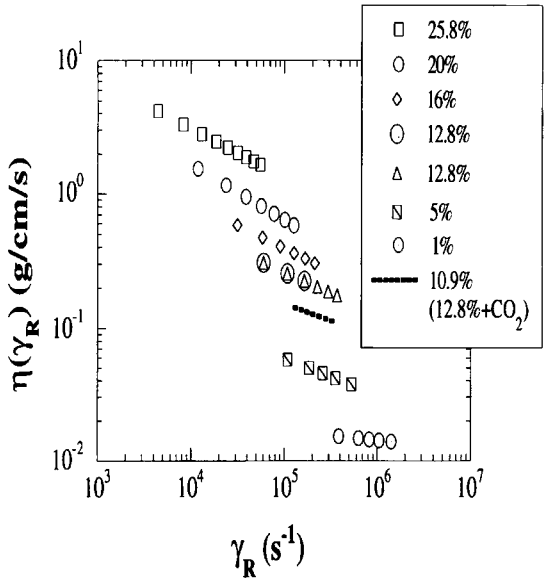

Figure 4 Non-Newtonian viscosity at the capillary wall as a function of shear rate and polystyrene concentration in toluene (22°C).

Table I Parameters for the Power-law Equation [Eq. (1)] for Solutions of Polystyrene in Toluene at 22°C

Wt % Polystyrene	m (g/cm/s)	n
1	0.0407	0.9241
5	1.4585	0.7222
12.8	9.1910	0.6909
16	20.193	0.6579
20	74.017	0.5876
25.8	89.627	0.6347

ical point, at a constant temperature and pressure (see Table II). At a sufficiently large pressure, only a one-phase liquid solution is present. For a given polymer concentration in pure toluene, the addition of CO_2 lowers the cohesive energy density and eventually precipitates the polymer.[24] Notice that significant amounts of CO_2 may be added (up to 34%), while remaining in the one-phase region. At higher polymer concentrations, a smaller amount of CO_2 causes phase separation, as expected.

Precipitation: From Polymer Discrete to Polymer Continuous Regions

In this section, the PCA process is used to produce a broad variety of morphologies for polymer concentrations ranging from 1 to 25.8 wt %. The emphasis is on concentrations where polymer continuous fibers are formed. The next section focuses on the region where spinodal decomposition is most prevalent.

By spraying 0.1–2.5 wt % polystyrene in toluene solutions, which are below the estimated critical composition of approximately 3 wt %,[3] polymer microspheres are formed. As shown in Figure 5, the primary spheres are fairly uniform in size and are extremely small, typically 100 nm in diameter. A light, airy, and loosely flocculated macrostructure is observed with a cobweblike appearance. The ability to form such small microspheres by a purely physical phase separation technique is rare. The formation mechanism is likely polymer nucleation and growth in a solvent-rich phase.

Submicron spheres are formed over a temperature range of 0–25°C. As the temperature is increased, the spheres agglomerate to form particles an order of magnitude larger, due to plasticization of the polymer by CO_2.[15]

Even for these very dilute solutions, part of the phase separation may be due to spinodal decomposition (Fig. 1). The more rapidly the mass-transfer pathway passes through the metastable region, the greater the importance of spinodal phase separation. By using an approximation of a solution presented by Crank,[27] the time scale for diffusion loss of toluene from spherical droplets can be estimated by:

Table II Liquid-phase Composition (Weight Fraction Units) at the Onset of Phase Separation for the System Polystyrene–Toluene–CO_2 at 22°C and 60.6 Bar

CO_2	Polystyrene	Toluene
0.4	0.006	0.594
0.35	0.0379	0.612
0.34	0.0845	0.575

$$t_{1/2} \sim \frac{0.02182a^2}{D} \qquad (2)$$

where $t_{1/2}$ is defined as the time to lose half of the toluene (or half-time). Assuming a diffusivity (D) of toluene in a toluene solution of $\sim 10^{-5}$ cm^2/s and a droplet diameter ($2a$) of 0.5 μm, the half-time for toluene loss is approximately 10^{-6} s. For a 10 μm droplet, this time would increase by a factor of 400. Convection would shorten this time. Because of this very rapid mass-transfer, spinodal decomposition may play a role.

Previously, it was proposed that rapid atomization of the liquid jet in dense CO_2, followed by rapid drying of the droplets, leads to the small particles.[15] At these low concentrations, the solutions are estimated to be close to the dilute solution region.[28] where the polymer chains in solution do not overlap.

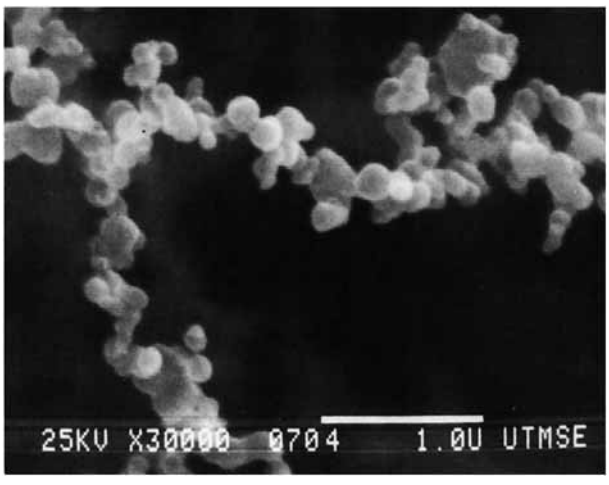

Figure 5 SEM photograph of polystyrene microspheres formed by spraying a 2.5% polystyrene in toluene solution through a 100 μm nozzle into CO_2 at 22°C, 0.786 g/cc, 70 bar, and a ΔP across the nozzle of 55 bar. After toluene was purged from the cell, the temperature was raised to 32°C and depressurized.

It is likely that the solution concentration is not high enough to cause significant delay in chain untangling, and, as well, the concentration is below the critical composition. Thus, the observed morphology is discrete polymer spheres.

At a higher polystyrene concentration of 3.5%, a slightly different macrostructure is formed at 25°C (see Table III). Overall, it is an open, airy fiber, 100–200 μm in diameter, that appears to be composed of very small subfibers (100–200 nm diameter and 0.2–5 μm long) that break easily upon handling. The structure is more connected than expected merely by flocculation of microspheres. The primary fibers are composed of 100–200 nm spheres that are fused end-to-end to form short fibers in a three-dimensional network. Because the solution is now in the semidilute region, chain entanglements increase the solution viscosity and likely cause kinetic limitations for the formation of discrete polymer microspheres.

At an initial polymer composition of 5% and over the temperature range of 10–40°C, fibers are formed, as shown in Figure 6 for a temperature of 30.5°C. Continuous fibers many centimeters long are formed (which is also the case for all of the fibers described below). These fibers in Figure 6 are not uniform, nor do they contain a single skin; rather they are composed of many smaller 1 μm diameter fibrils. Previously, a 5% solution sprayed into carbon dioxide at 22°C and 0.74 g/cc formed ~20 μm solid fibers for a ΔP of 55 bar.[15] The slightly higher temperature and much larger ΔP (172 bar) in Figure 6 causes

Table III Observed Polymer Morphology Produced by Spraying a Polystyrene in Toluene Solution into an Antisolvent

T (°C)	P (bar)	CO_2 Density (g/cc)	Wt % Polymer	ΔP Across Nozzle (bar)	Microstructure	Macrostructure
22	70	0.786	2.5	55[a]	~ 100 nm microspheres, flocculated	"Cobweblike"
25	80.3	0.778	3.5	55[a]	0.1–0.2 μm i.d. subfibers	100–200 μm porous fiber
22	62.4	0.74	5	55[a]	~ 20 μm solid fiber	Solid fiber
30.5	73	0.583	5	172.3[a]	~ 1 μm oriented subfibers	100–200 μm porous fiber
22	70	0.786	8	34	~ 10 μm walls with 1–5 μm pores	200–300 μm hollow fiber
22	70	0.786	10	69	~ 10–15 μm walls with 1–5 μm pores	100–150 μm hollow fiber
22.5	70	0.78	12.8	69	1–20 μm asymmetric pores	~ 185 μm porous fiber
22.5	70	0.78	16	69	1–12 μm asymmetric pores (oval pores near surface)	~ 200 μm porous fiber
22	70	0.786	20	137.9	1–8 μm slightly asymmetric pores (oval pores near surface)	~ 150 × 300 μm ribbonlike fiber
22	70	0.786	25.8	241.3	1–4 μm uniform pores (oval pores near surface)	~ 100 × 300 μm ribbonlike fiber
22	70	0.786	8	68	~ 1–6 μm porous walls and submicron interconnected regions	~ 150 μm hollow fibers and ~ 200–250 μm airy fibers
0.2	53	0.942	8	69[b]	Submicron interconnected network	Airy fiber
0.2	46.5	0.937	10	69[b]	Submicron interconnected network	~ 150 μm airy fiber
0.2	46.5	0.937	10	206.8[b]	0.2–1 μm oriented fibrils	~ 150 μm airy fiber
22	70	0.786	10.85[c]	69	~ 10–15 μm walls with 1–5 μm pores	100–200 μm hollow fibers
22	70	0.786	15.9[d]	69	1–15 μm pores (no oval pores near surface)	~ 110–180 μm porous fiber
22	1	[e]	12.8	65.5	Slight porosity, 0.5–3 μm pores	~ 150 μm irregular-shaped fiber

Unless otherwise noted, the solution was sprayed through a 151 μm i.d. × 18 cm-long capillary tube into a vertical cell (Fig. 3) containing compressed CO_2.

[a] 100 μm i.d. × 17.4 cm-long nozzle in a horizontal-view cell.

[b] In a horizontal-view cell.

[c] 15.2 wt % (total wt basis) CO_2 preadded to a polystyrene solution before spraying.

[d] 20.7 wt % (total wt basis) CO_2 preadded to a polystyrene solution before spraying.

[e] Into liquid methanol.

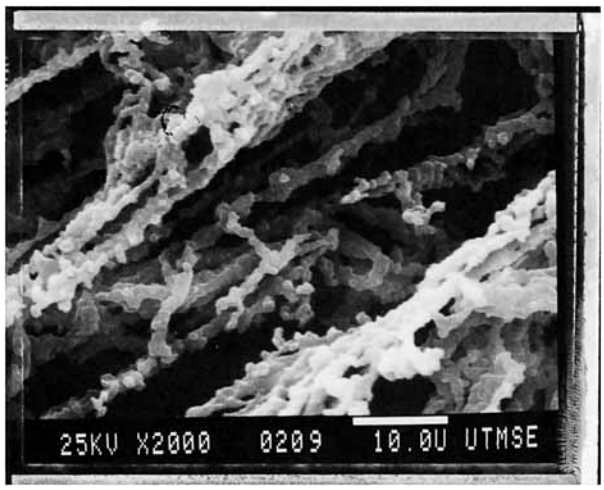

Figure 6 SEM photograph of polystyrene subfibers formed by spraying a 5% polystyrene in toluene solution through a 100 μm nozzle into CO_2 at the following conditions: 30.5°C, 0.583 g/cc, and 73 bar. ΔP =172.3 bar.

some breakup of the liquid jet, resulting in many smaller subfibers. These fibrils are highly oriented in the jet. The 5% solution is now in the semidilute region where there is significant chain entanglement. This entanglement is evident due to the increased solution viscosity at constant shear rate. At 5%, the solution viscosity increases ~ 227% compared with the 1% solution, i.e., 0.055 g/cm/s vs. 0.0168 g/cm/s. The shift toward a polymer continuous morphology is apparent; however, solvent voids are not yet observed in the micrographs. It is likely the mass-transfer pathway still crosses the binodal curve below the critical composition. Thus, the polymer discrete morphology is due to polymer nucleation and growth within a solvent-rich continuous region.

Increasing the polystyrene composition to 8% at 22°C produces a hollow fiber that has a well-defined cylindrical shape and a skin on the surface (Fig. 7). Here, the solution was sprayed into the vertical cell, with a lower ΔP of 34 bar. To obtain a photograph of the fiber cross-section, a fiber was immersed in liquid nitrogen, removed, and immediately cut with a new razor blade. It was attached to a scanning electron microscope (SEM) stage, and the results indicate that the fibers are approximately 200–300 μm in diameter. This diameter is significantly larger than the inside diameter of the nozzle, which is 151 μm. It is likely that the viscoelastic forces in the polymer solution cause some die-swell to occur.[29] Also, CO_2 mass-transfer rates into the liquid jet are considerably larger than are the toluene transfer rates out. This difference could cause fiber swelling prior to vitrification. The mass-transfer differences will be discussed below in more depth.

As the 8% solution is sprayed into liquid CO_2, the jet is stabilized by the larger solution viscosity (relative to more dilute solutions).[30] Additional stability is obtained on the surface of the jet by a rapid increase of the surface viscosity, due to the rapid mass-transfer of toluene and carbon dioxide. In fact, a precipitated polymer skin may form on the jet surface, which would also inhibit breakup. At a given viscosity, mathematical models have shown that a viscoelastic jet tends to be less stable than is a Newtonian jet.[31,32] However, these models did not address the more complex case of mass-transfer into and out of the jet, as well as the effects of skin formation.

Several diffusion coefficients are needed for the calculations below. The diffusion coefficient of dilute toluene through amorphous (glassy) polystyrene is estimated at 25°C to be on the order of 10^{-13} cm^2/s.[17] For more concentrated toluene in polystyrene, the coefficient could be as high as 10^{-9}. This value is still two orders of magnitude below that of CO_2 in polystyrene, which is 10^{-7} cm^2/s.[19] The diffusion coefficient of toluene in CO_2 is on the order of 10^{-4} cm^2/s.[33]

Pinnau,[6] Strathmann and Kock,[5] and others have suggested that a rapid loss of solvent from the surface of a polymer solution creates an increased polymer concentration, leading to rapid precipitation and formation of a dense skin. It is instructive to estimate semiquantitatively how long it would take to lose toluene from, say, the outer 2 μm of the liquid jet. We assume that this diffusion is through pure CO_2, and neglect convection, which would enhance toluene loss from the jet. The diffusion coefficient will decrease in this outer region as the polymer

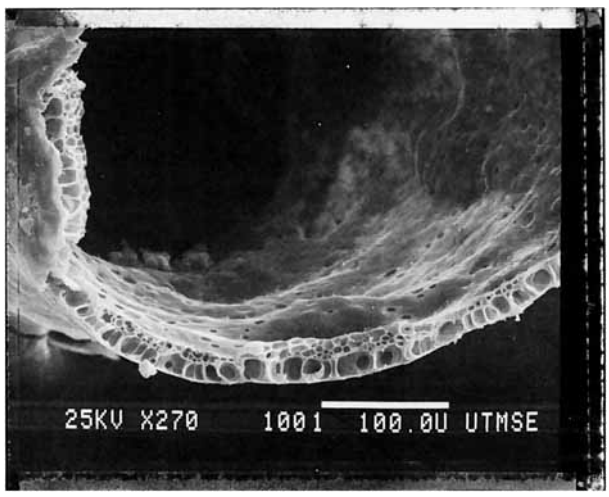

Figure 7 SEM photograph of a polystyrene hollow fiber formed by spraying a 8% polystyrene in toluene solution through a 151 μm nozzle into CO_2 at the following conditions: 22°C, 0.786 g/cc, and 70 bar. ΔP = 34 bar.

concentration increases, but this complex behavior will be neglected for the qualitative arguments below. Again, using an approximate solution from Crank,[27] the calculated time to lose toluene in the outer 2 μm is estimated to be 3×10^{-4} s. For a typical jet velocity of 220 cm/s, the fluid would travel 0.068 cm or $\sim$ 4.5 jet diameters in this time period. This length may be compared to the jet breakup length to explain the morphology.

The jet breakup length depends upon the interfacial tension of the polymer solution in CO_2. The interfacial tension varies throughout the jet due to the variation in composition. There are experimental difficulties in obtaining accurate values of interfacial tensions at high pressures for such a system. Since the interfacial tension is unknown, precise breakup lengths cannot be calculated. However, we will now show that the morphologies of several of the above fibers are consistent with expectations based on the length the jet travels during the time period for loss of surface toluene. This approach is somewhat simplified, e.g., since the viscosity in the core of the jet may also influence the breakup.

For the case of a 5% polystyrene solution, the jet would travel $\sim$ 4 jet diameters at a velocity of 132 cm/s during loss of surface toluene for a 100 μm diameter nozzle.[15] The observed formation of a single-strand fiber indicates that the jet did not breakup. For an 8% polystyrene concentration (Fig. 7), the velocity is slightly lower (101 cm/s) and the estimated length of jet travel during skin formation is $\sim$ 2 jet diameters. Again, the resulting morphology is a single-strand fiber. In these two examples, the rapid formation of a dense skin counteracts any tendency for the jet to breakup, even in the dense CO_2 environment. In contrast, for considerably more dilute solutions, the viscosity is sufficiently low such that the jet breaks up to form microspheres before a skin is formed.

If the jet velocity for a 5% solution is increased to 580 cm/s (Fig. 6), the jet must travel about 17 jet diameters before the surface toluene is lost. The jet has time to begin to breakup, as suggested by the formation of many smaller diameter fibrils. However, because the viscosity builds quite rapidly as toluene leaves, and this solution is in the semidilute region, the polymer chains cannot fully untangle before the polymer solidifies. Consequently, the many small fibrils are interconnected or intertwined to form a single macroscopic fiber.

We now present a mechanism to explain the formation of the hollow fibers. Within a few diameters from the capillary tip, a skin forms in the jet as explained above, which restricts diffusion. Clearly, CO_2 diffuses through this glassy skin faster than does toluene, based on diffusion coefficients listed above. As more and more CO_2 diffuses into the jet, the phase-separation interface between polymer and solvent moves further toward the center. The interior of the jet remains rich in toluene, because of its slow diffusion relative to CO_2. Thus, the polymer-rich domains will remain plasticized for some time, allowing the CO_2-rich voids to grow. These voids may coalesce as the wet polymer webs rupture. With sufficient time before vitrification, this growth and coalescence will lead to a hollow structure, with a porous shell, as observed. It is also possible that the fiber is expanded by the faster transfer of CO_2 into the liquid jet vs. that of the leaving toluene.

For the hollow fiber in Figure 7, the polymer shell is approximately 10–20 μm thick with 1–5 μm pores. The outer skin appears to be fairly defect-free, with no visible pores down to $\sim$100 nm or slightly smaller. However, this is just an observation made from the SEM and the SEM micrographs; smaller possible defects could be investigated with permeability studies.

For a 10% polystyrene concentration, hollow fibers are also formed with a shell thickness of 10–15 μm, with 1–5 μm pores (Table III).[4] As the polystyrene concentration is raised to 12.8% the resultant fiber is now fully porous and no longer hollow (Fig. 8). The pore structure appears to be slightly asymmetric with the larger pores toward the center of the fiber. This asymmetry may be explained as discussed above, namely, the center stays wet with toluene slightly longer allowing for more coalescence of some of the interior solvent–antisolvent voids.

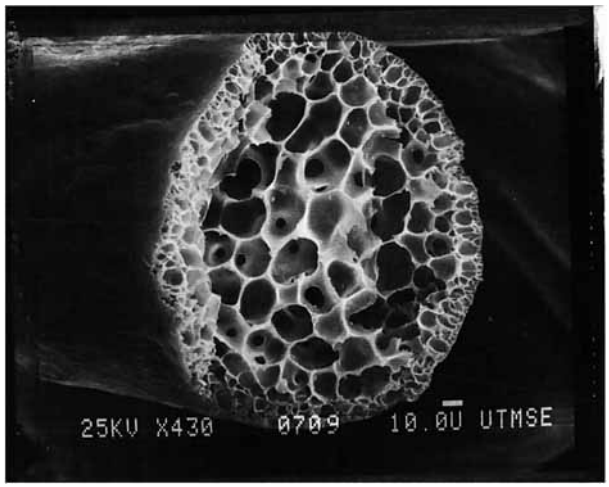

Figure 8 SEM photograph of a polystyrene fiber formed by spraying a 12.8% polystyrene in toluene solution through a 151 μm nozzle into CO_2 at the following conditions: 22.5°C, 0.78 g/cc, and 70 bar. ΔP = 69 bar.

By careful inspection of Figure 8, small openings can be seen inside some of the central pores. These openings suggest the polymer web was beginning to rupture between two voids just before the morphology was vitrified.

The cell density, or number of voids per cm^3 of foam (N_f) can be estimated from a SEM micrograph by the following equation[34]:

$$N_f = \left(\frac{n_v M^2}{A}\right)^{1.5} \quad (3)$$

where n_v is the number of voids in an area of A cm^2 (area of interest on micrograph) and M is the magnification of the micrograph. From Figure 8, the cell density is estimated at 3×10^{10}. This cell density is over 2 orders of magnitude higher than those reported by Kumar and Suh,[34] based on foaming with N_2.

With an additional increase in polystyrene concentration to 16% (Fig. 9), the pore structure appears to be more uniform and is less porous. Increasing the composition to 20% (Fig. 10), and even to 25.8%,[14] indicates that this trend continues. One explanation for this trend can be seen on Figure 2. As the starting polymer composition is increased, assuming that the mass-transfer pathways retain the same shape, the ending composition will also increase, leading to lower porosity. A second reason is that the solution viscosity increases rapidly as the polymer concentration increases (goes as the fourth power of concentration), which likely inhibits, or even prevents, growth and coalescence of the pores.

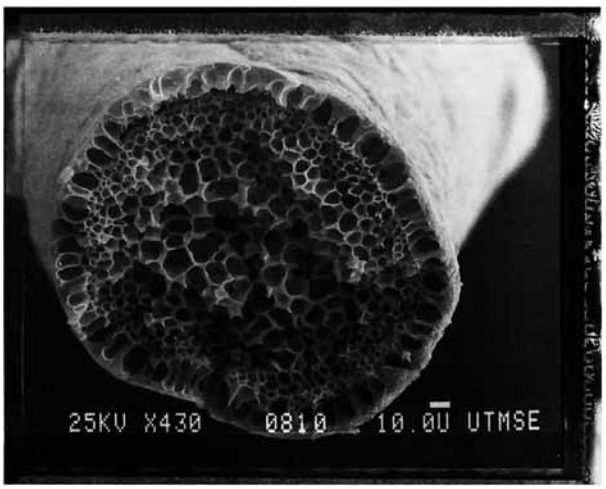

Figure 9 SEM photograph of a polystyrene fiber formed by spraying a 16% polystyrene in toluene solution through a 151 μm nozzle into CO_2 at the following conditions: 22.5°C, 0.78 g/cc, and 70 bar. ΔP = 69 bar.

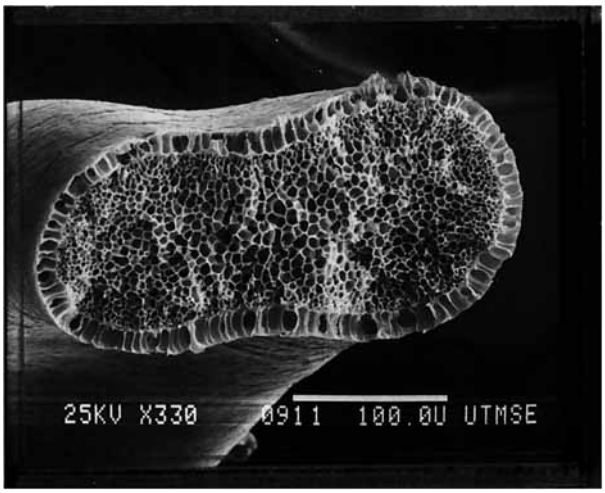

Figure 10 SEM photograph of a polystyrene fiber formed by spraying a 20% polystyrene in toluene solution through a 151 μm nozzle into CO_2 at the following conditions: 22°C, 0.786 g/cc, and 70 bar. ΔP = 137.9 bar.

The fiber shown in Figure 10, for 20% polystyrene, is ribbonlike with an approximate 1:2 aspect ratio. Although the exact cause of this is not known, it is likely that the fiber has exceeded a stable diameter and has begun to divide into two fibers. With more polymer present, the mass-transfer rates of toluene and CO_2 will be lower, causing the fiber to remain wet longer, providing additional time for this separation. The same behavior is observed with a 25.8% polystyrene solution.

Spinodal Region

Based on the above results, it is obvious that a transition from polymer discrete to polymer continuous morphology occurs for an initial polystyrene concentration between 3.5% and 10 wt %. We focus on this transition region, where it should be possible to cause a rapid spinodal decomposition. From Table II, it is estimated that the critical composition is in the range of 5% polystyrene. Here, the metastable region is small, and spinodal decomposition is easily attained (see path B in Fig. 1). Smolders[35] reported that spinodal decomposition is highly improbable in the liquid antisolvent-induced phase separation for membranes, because nucleation and growth kinetics are too fast to allow penetration into the spinodal region. This statement applies to high polymer concentrations used in membrane formations. However, at lower concentrations near the ternary critical composition, a deep, rapid quench should be sufficient to cause phase separation by spinodal decomposition. Also, as discussed below, CO_2 mass-transfer

rates are faster in glassy, amorphous polymers than are conventional liquid antisolvents.

One way to speed up phase separation and vitrification (i.e., to quench a solution more rapidly) is to enhance mixing of the toluene and CO_2 through increased convective mass-transfer. This was attempted by spraying an 8% solution at increased flow rates. Previously, at an 8% composition (Fig. 7), a hollow fiber was produced with a ΔP of 34 bar. Doubling the ΔP to 68 bar results in some hollow fibers.[14] However, there are also interconnected fibers with bicontinuous curvatures, suggesting that it is possible for an 8% solution to access the spinodal region. It is conceivable that an even more rapid and complete quench could be used to completely avoid producing hollow fibers.

Based on previous work showing the effect of temperature on PCA,[15] it appeared to be interesting to spray solutions into cold CO_2, well below 25°C. At reduced temperatures, mass-transfer rates as well as nucleation and growth kinetics are slower. These factors would make phase separation less likely prior to crossing the spinodal. Also, the polymer glassy region is expanded. Thus, the morphology can be frozen-in sooner, minimizing coarsening.

Figure 11 is a result of spraying an 8% polystyrene solution into ~0°C CO_2 with a ΔP of 69 bar. An interconnected network of polymer and voids is formed, likely by spinodal decomposition. However, one must be cautious in assigning a phase-separation mechanism based solely on final morphology. The macrostructure is still a fiber due to the process of spraying through a nozzle; however, the substructure

Figure 11 SEM photograph of polystyrene morphology formed by spraying a 8% polystyrene in toluene solution through a 151 μm nozzle into CO_2 at the following conditions: 0.2°C, 0.942 g/cc, and 53 bar. ΔP = 69 bar.

is very different from that observed at 22°C. The primary polymer dimensions are submicron. This new technique offers the potential to form high surface area materials. For example, if the polymer regions in Figure 11 are averaged as 100 nm cylinders, then the surface area is estimated as 40 m^2/g. It may be possible for the individual polymer domains to be porous, leading to even higher surface areas, although measurements of internal surface area have not been performed. Aubert and Sylwester[3] formed structures very similar in appearance to Figure 11, most likely by spinodal decomposition.

For a 10% polystyrene concentration, the metastable region is still sufficiently narrow so that a large part of the phase separation could occur by spinodal decomposition. Again, solutions were sprayed into 0°C CO_2 to quench rapidly into the spinodal region. An example result (Fig. 12) shows that interconnected polymer and void regions are formed. It appears that the polymer volume fraction is larger than in Figure 11, as expected due to the higher concentration. In addition, the polymer domains are more connected. The presence of a few large voids suggests that some phase separation took place in the metastable region, or that coarsening occurred after spinodal decomposition and before vitrification.

Based on the above interesting results with higher flow rates for the 8% solution, a second set of experiments was performed for a polystyrene concentration of 10% at 0°C. The ΔP across the nozzle was increased from 69 to 207 bar to determine if faster jet breakup could cause the mass-transfer pathway to reach the spinodal curve sooner. Although the macrostructures of the fibers at the two different flow rates looked similar,[14] the substructures were significantly different. For the higher ΔP, the fiber is composed of many small fibrils (Fig. 13). The diameters of the fibrils are similar to those of the primary polymer particles in Figure 12. These fibrils are oriented primarily along the axis of the macrofiber, suggesting that a fine microstructure is formed by spinodal decomposition, as before, and then this structure is oriented in the high shear of the jet. Larger surface areas result from low interfacial tensions, and coarsening is minimized by rapid quenching at low temperature.

Lele and Shine[10] showed, in some cases, that RESS formed 1–5 μm fibers with a 50 μm restrictor. For comparison, the fibers in Figure 13 are an order of magnitude smaller. It is interesting that these small fibers were produced by spraying through a nozzle three times the size of a typical RESS nozzle and that the polymer concentration was approximately two orders of magnitude higher. This spi-

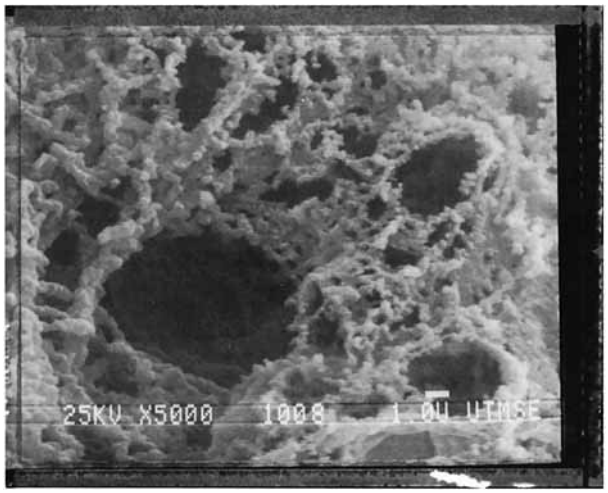

Figure 12 SEM photograph of polystyrene morphology formed by spraying a 10% polystyrene in toluene solution through a 151 μm nozzle into CO_2 at the following conditions: 0.2°C, 0.937 g/cc, and 46.5 bar. ΔP = 69 bar.

nodal morphology is also quite different than that obtained by Aubert and Sylwester[3] because of the orientation caused by the capillary. In the TIPS process, phase separation occurs while the polymer solution is quiescent, in contrast to the PCA process, which by nature is a flow process.

Antisolvent Addition Prior to Spraying

The addition of antisolvent to the feed alters the mass-transfer pathway as shown in Figure 2. As shown, path [d] begins at a point closer to the binodal curve than does path [c]. The mass-transfer pathway shifts away from the polymer vertex toward the antisolvent vertex, resulting in a more porous polymer. The phase equilibrium results in Table II were used to determine the amount of CO_2 that may be added to a polystyrene-toluene solution at room temperature without phase separation. This amount is approximately 35 wt % CO_2.

CO_2 was added in varying amounts, from 1 to 21 wt %, to a 1 wt % polystyrene in toluene solution. No change in particle size was observed, as shown in Table IV, for the temperature range 10–23°C. For this dilute solution, a polymer-rich phase nucleates and grows to form discrete polymer microspheres. At the highest concentration of CO_2 addition (21%), the polymer solution is diluted to 0.79 wt % polystyrene. However, the same size (100 nm) microspheres are formed. At 35°C, plasticization of polystyrene by CO_2 causes agglomeration, in agreement with previous results.[15]

Experiments were done with an ~0.1 wt % polystyrene in toluene solution without any added CO_2, to see if more dilute solutions would result in smaller microspheres. As Table IV indicates, the microspheres are still ~100 nm in diameter. It is likely that the penalty to form smaller particles with more surface area is too high.

Next, 15.2 wt % CO_2 (based on the final total solution weight) was added to a 12.8% polystyrene in toluene solution. The polymer concentration after CO_2 addition was calculated as 10.85 wt %. This solution was sprayed into liquid CO_2 at 22°C. The resultant morphology (not shown) is a 100 μm diameter hollow fiber, with a shell approximately 10–15 μm thick containing 1–5 μm pores.[14] The added CO_2 causes the fiber to be more porous, as expected. However, the fiber is nearly identical to that obtained with a 10% polystyrene solution containing no preadded CO_2. The fact that CO_2 lowers the viscosity more than does toluene, for a given weight, does not appear to change the morphology or porosity. Preadded CO_2 appears to act in the same manner as does a liquid diluent in this example.

A 15.9 wt % polystyrene in toluene/CO_2 solution was made by adding 20.7 wt % CO_2 to a 20% polystyrene in toluene solution. This solution was also sprayed into liquid CO_2 at 22°C, resulting in porous fibers with average diameters of 175 μm containing 1–15 μm uniform pores (not shown).[14] These fibers are very similar to the those formed from a 16% polystyrene solution without preadded CO_2 (see Figure 9). The only noticeable difference is that these fibers do not have oval pores near the surface, as is the case in Figure 9. Thus, in this case, somewhat different results are obtained with preadded CO_2 compared with a liquid diluent.

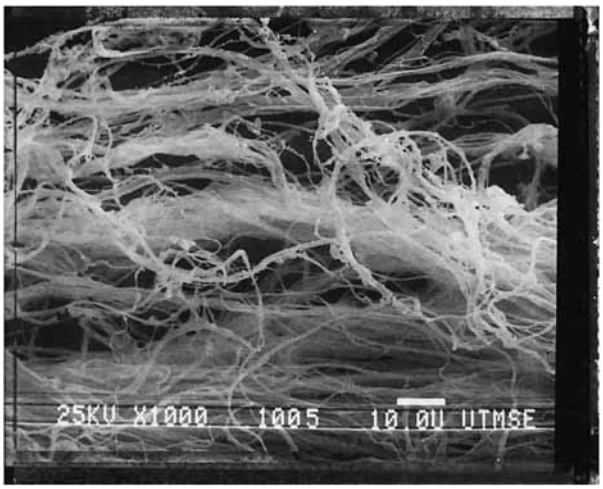

Figure 13 SEM photograph of polystyrene fibrils formed by spraying a 10% polystyrene in toluene solution through a 151 μm nozzle into CO_2 at the following conditions: 0.2°C, 0.937 g/cc, and 46.5 bar. ΔP = 206.8 bar.

Table IV Observed Polymer Morphology Produced by Spraying a Polystyrene in Toluene Solution into Carbon Dioxide

T (°C)	P (bar)	CO_2 Density (g/cc)	Wt % CO_2 Preadded	Primary Particle Diameter (μm)	Microstructure	Macrostructure
22.5	63.4	0.757	5	~ 0.1	Microspheres, flocculated	"Cobweb"
35	85.9	0.626	5	1–2	Microspheres, agglomerated 10–20 μm groups	Powder
10.1	45.8	0.863	21[a]	~ 0.1	Microspheres, flocculated	"Cobweb"
10	46.9	0.864	0[b]	~ 0.1	Microspheres, flocculated	Powder
10	46.9	0.864	0[a,b]	~ 0.1	Microspheres, flocculated	Powder

Unless otherwise noted, a 1 wt % solution was sprayed through a 100 μm i.d. × 17.4 cm-long capillary tube at a constant differential pressure of 55 bar.

[a] ΔP = 138 bar.

[b] 0.097 wt % polystyrene solution.

Methanol as an Antisolvent

To place the results of this study in perspective, experiments were performed with liquid methanol as the antisolvent instead of CO_2. Methanol is a common antisolvent for polystyrene.[36] A 12.8 wt % polystyrene in toluene solution was sprayed into liquid methanol at 22°C. The nozzle was immersed in the liquid, and the differential pressure across the nozzle was 65.5 bar. Fibers were formed, which by visual observation phase-separated (became opaque) 7–10 times slower than did polystyrene fibers quenched in liquid CO_2. The resultant fibers have a similar overall diameter of ~150 μm, but have an irregular shape (Fig. 14). In some respects, the shape is similar to Figure 10 in that the fiber is beginning to break into several smaller diameter fibers. This may suggest that while the liquid polymer thread is stable to typical Rayleigh instabilities it is not stable to radial instabilities.

It is obvious from Figure 14 that the polymer is not as porous as those produced with CO_2. From a micrograph with higher magnification,[14] the cell density was estimated as 6×10^{11}, about an order of magnitude higher than for the same solution sprayed into liquid CO_2 (Figure 8). The fiber precipitated with CO_2 has a lower cell density due to the growth and coalescence of the interior pores, whereas in the case of precipitation with methanol, not as much growth occurs. This coalescence, or lack thereof, is especially evident in the center of the fiber. The growth also manifests itself as pore asymmetry. The CO_2 precipitated fiber has a slightly asymmetric pore structure whereas the methanol precipitated fiber does not.

The porosity in Figure 14 was estimated by the method of Kumar and Suh[34] to be 0.007, or one to two orders of magnitude less than that obtained by PCA with CO_2. This reduced porosity indicates that the mass-transfer path is different from the path followed when CO_2 was used as the antisolvent. Two scenarios will be considered to explain the porosities.

Assuming that only liquid is present in the jet (in other words, the polymer has not yet formed a dense skin), then it would be expected that the transfer of toluene from the jet into the methanol continuous phase would be slower than into CO_2, based on the order of magnitude difference in diffusion coefficients.[33] The transfer of either methanol or CO_2 into the polymer solution in the jet would be expected to be similar, since the diffusivities of either antisolvent in toluene is approximately the same ($\sim 10^{-5}$ cm^2/s). According to this scenario, the pathway for methanol would be more like case [a]

Figure 14 SEM photograph of a polystyrene fiber formed by spraying a 12.8% polystyrene in toluene solution through a 151 μm nozzle into liquid methanol at 22°C and with a ΔP = 65.5 bar.

in Figure 2, whereas that of CO_2 would be more like case [c]. A denser fiber would be produced in CO_2, the opposite of the observed result.

A second scenario is proposed in which a dense skin forms rapidly and acts as a barrier. Here, the relative diffusion rate of each of the antisolvents through this skin becomes extremely important. As previously mentioned, the diffusivities of methanol and CO_2 in amorphous polystyrene are $\sim 10^{-9}$ and $\sim 5 \times 10^{-7}$ cm^2/s, respectively. The time scale ($t_{1/2}$) for transfer of methanol into a liquid cylindrical jet (151 μm in diameter) is ~23 min, and for CO_2, ~5.6 seconds. Thus, CO_2 transfers into the interior of the jet much faster and can initiate precipitation quicker. For example, CO_2 will precipitate and vitrify the top 2 μm of the jet (as discussed earlier) an order of magnitude faster. For jet velocities of 220 cm/s, the methanol precipitated jet will have to travel 44 jet diameters, compared to 4.5 for the CO_2 precipitated case, to remove the surface toluene. Since CO_2 initiates precipitation faster, the cells in this fiber will have more time to grow (while sufficient toluene is still present) before the morphology is vitrified. Because of this growth, the cell density will decrease. In the case of methanol, less toluene is present in the interior during growth of the voids. Consequently, the polymer becomes stiff, keeping the cells small and uniform, and the resulting porosity is low. To form more porous fibers with methanol, different experimental conditions would be required.

CONCLUSIONS

Compressed CO_2 is an effective antisolvent, providing the ability to control final polymer morphology over a continuum from microspheres to interconnected bicontinuous networks to fibers. Extremely small 100 nm microspheres, which are difficult to form by a purely physical phase-separation technique, are obtained at concentrations below 3.5 wt % polystyrene in toluene. The sprayed liquid jet atomizes rapidly, producing small droplets that are quickly dried due to rapid loss of toluene. The primary precipitation mechanism in this region is likely nucleation and growth of polymer in a solvent-rich continuous phase, however, some spinodal decomposition can also be present.

At polymer concentrations in the vicinity of the critical composition, between 3.5 and 8% polystyrene, there exists a transition region where neither discrete polymer microspheres nor single-strand fibers are produced. The high solution viscosity, coupled with the high polymer concentration, stabilize the liquid jet, providing kinetic limitations to the untangling of chains. At even higher polymer concentrations (8%–26%), the solution viscosity increases dramatically. The stabilization of the liquid jet by viscous forces, in conjunction with a rapid loss of toluene from the surface of the jet, leads to formation of single-strand fibers with a skin. The proposed formation of a dense surface skin on the fibers creates a diffusion-limiting barrier. The rapid diffusion of CO_2 into glassy amorphous polystyrene, coupled with the slower loss of toluene, creates fibers that are porous and, in some instances, even hollow. The porosity and/or size of the hollow core may be controlled, and both are inversely proportional to the initial polymer solution concentration. The mechanism for phase separation in this region is nucleation and growth of CO_2-rich cells within a polymer continuous phase, forming microcellular foams with pores sizes ranging from 1–20 μm.

When quenching the 8 and 10% polystyrene solutions rapidly (high ΔP at 0°C), it is likely that much of the phase separation is by spinodal decomposition. Precipitation in this region results in an interconnected, bicontinuous polymer-void network, typical of spinodal decomposition. The most rapid quenches in this work were obtained at ~0°C, where it is proposed that the polymer-rich phase intersects the T_g curve sooner. Here, coarsening prior to vitrification is minimal. At very high shear rates, highly oriented submicron fibrils are formed due to spinodal decomposition, low interfacial tension, and rapid quenching.

CO_2 when added to the polymer solution prior to spraying, acts as a diluent. Solutions of polystyrene, toluene, and CO_2 exhibit shear thinning behavior for the shear rates studied. CO_2 adds free-volume into the polymer solution, leading to a beneficial reduction in the solution viscosity, greater than in the case of liquid diluents. In some cases, the preadded CO_2 produces the same morphology as for a conventional liquid diluent, whereas in other cases, changes in morphology are present.

The efficacy of CO_2 as an antisolvent relative to methanol is influenced by the widely different mass-transfer rates. The diffusion coefficient of CO_2 in the glassy polystyrene skin is one to two orders of magnitude higher than that of methanol. Consequently, the porosity is higher for CO_2 and there is a greater tendency to preserve the cylindrical fiber shape.

Acknowledgment is made to Gabriel Luna-Bárcenas, Don Paul, Bill Koros, and Robert Schechter for many helpful discussions. Also, acknowledgment is made to the Separations Research Program at the University of Texas, the

State of Texas Energy Research in Applications Program, and the Camille and Henry Dreyfus Foundation for a Teacher-Scholar Grant (to K. P. J).

REFERENCES

1. D.R. Lloyd, K. E. Kinzer, and H. S. Tseng, *J. Membrane Sci.*, **52**, 239 (1990).
2. F. Tsai and J.M. Torkelson, *Macromolecules*, **23**, 775 (1990).
3. J. H. Aubert and A.P. Sylwester, *Chemtech*, **May, 290** (1991).
4. D. R. Lloyd, S. S. Kim and K. E. Kinzer, *J. Membrane Sci.*, **64**, 1 (1991).
5. H. Strathmann and K. Kock, *Desalination*, **21**, 241 (1977)
6. I. Pinnau, PhD dissertation, University of Texas at Austin, Austin, TX, 1991.
7. V. J. Krukonis, Paper 140f, AICHE Meeting, San Francisco, Nov., 1984.
8. D. W. Matson, J. L. Fulton, R. C. Petersen, and R. D. Smith, *Ind. Eng. Chem. Res.*, **26**, 2298 (1987).
9. J. W. Tom, and P. G. Debenedetti, *J. Aerosol Sci.*, **22**, 555 (1991).
10. A. K. Lele and A. D. Shine, *AICHE J.*, **38**, 742 (1992).
11. X. Kwauk and P. G. Debenedetti, *J. Aerosol Sci.*, to appear.
12. J. S. Colton and N. P. Suh, *Polym. Eng. Sci.*, **27**, 493 (1987).
13. S. W. Cha and N. P. Suh, *ANTEC '92*, 1527 (1992).
14. D. J. Dixon, PhD dissertation, University of Texas at Austin, Austin, TX, 1992.
15. D. J. Dixon and K. P. Johnston, *AICHE J.*, **39**, 127 (1993).
16. T. W. Randolph, A. D. Randolph, M. Mebes, and S. Young, to appear.
17. A. R. Berens and H. B. Hopfenberg, *J. Membrane Sci.*, **10**, 283 (1982).
18. M. A. McHugh and V. J. Krukonis, Supercritical Fluid Extraction Principles and Practice, *Supercritical Fluid Extraction: Principles and Paractice*, Butterworths, Stoneham, MA, 1986.
19. A. R. Berens and G. S. Huvard, Am. Chem. Soc. Symp. Ser. 406, American Chemical Society, Washington, DC, 1989, p. 207.
20. A. Garg, L. Gerhardt, E. Gulari, and C. W. Manke, in *ACS Preprints*, Vol. 233, American Chemical Society, Boston, MA 1990.
21. B. W. Müller, and W. Fischer, Ger. Patent Application DE 3,744,329 A1 (1989).
22. P. D. Condo and K. P. Johnston, *Macromolecules*, **25**, 6730 (1992).
23. H. Strathmann, P. Scheible, and R. W. Baker, *J. Appl. Polym. Sci.*, **15**, 811 (1971).
24. D. J. Dixon and K. P. Johnston, *AICHE J.*, **37**, 1441 (1991).
25. S. H. Page, S. R. Goates, M. L. Lee, D. J. Dixon, and K. P. Johnston, *J. Microcol. Sep.*, **3**, 355–369 (1991).
26. R. B. Bird, R. C. Armstrong, and O. Hassager, *Dynamics of Polymeric Liquids. Vol. 1 Fluid Mechanics*, Wiley, New York, 1977.
27. J. Crank, *The Mathematics of Diffusion*, Oxford University Press, New York 1975.
28. F. W. Billmeyer, Jr., *Textbook of Polymer Science*, Wiley, Inc., New York 1984.
29. Z. Tadmor and C. G. Gogos, *Principles of Polymer Processing*, Wiley, New York 1979.
30. R. P. Grant and S. Middleman, *AICHE J.*, **12**, 669 (1966).
31. S. Middleman, *Chem. Eng. Sci.*, **20**, 1037 (1965).
32. F. W. Kroesser and S. Middleman, *AICHE J.*, **15**, 383 (1969).
33. K. P. Johnston, *Encyclopedia of Chemical Technology*, 3rd ed., Suppl. Vol., New York, 1984, p. 872.
34. V. Kumar, and N. P. Suh, *Polym. Eng. Sci.*, **30**, 1323 (1990).
35. C. A. Smolders, in *Proceedings of the Symposium on Ultrafiltration Membranes and Applications*, Plenum Press, New York, 1980.
36. J. Brandrup, and E. H. Immergut, Ed., *Polymer Handbook*, 3rd. ed., Wiley, New York, 1989.

Received January 29, 1993
Accepted May 28, 1993